Dalton Transactions

ROYAL SOCIETY OF CHEMISTRY

PAPER

View Article Online
View Journal | View Issue

Cite this: *Dalton Trans.*, 2026, **55**, 3442

Synthesis, structural characterization and properties of a series of heteropolyoxomolybdates: $[AlMo_6(OH)_6O_{18}]^{3-}$, $[GeMo_{12}O_{40}]^{4-}$, $[GeMo_6O_{22}(Hmal)_3]^{7-}$, $[SiMo_{12}O_{40}]^{4-}$, and $[TeMo_6O_{24}]^{6-}$

D. Kuzman,*[a] V. Damjanović,[b] J. Toplak,[a] G. Medak,[c] I. Halasz,[d] T. Hrenar,[a] M. Cindrić*[a] and V. Vrdoljak[a]

Eight heteropolyoxomolybdates were synthesized and characterized, comprising three Anderson-type compounds $[Co(ox)(NH_3)_4]_3[AlMo_6(OH)_6O_{18}]\cdot 7H_2O$ (**1**), $[Co(ox)(NH_3)_4]_6[TeMo_6O_{24}]\cdot 16H_2O$ (**2**), and $Na_2[Co(ox)(en)_2]_4[TeMo_6O_{24}]\cdot 16H_2O$ (**3**), four Keggin-type compounds $[Co(ox)(NH_3)_4]_4[GeMo_{12}O_{40}]\cdot 6H_2O$ (**4**), $[Co(ox)(NH_3)_4]_4[SiMo_{12}O_{40}]\cdot 6H_2O$ (**5**), $[Co(ox)(en)_2]_4[GeMo_{12}O_{40}]\cdot 12H_2O$ (**6**), and $[Co(ox)(en)_2]_4[SiMo_{12}O_{40}]\cdot 12H_2O$ (**7**), as well as one coordination polymer $Na_4[Co(ox)(NH_3)_4]_3[GeMo_6O_{22}(Hmal)_3]\cdot 7.75H_2O$ (**8**) featuring an extensive three-dimensional coordination framework. Additionally, two reaction intermediates, $[\{Co(ox)(NH_3)_4\}_2Na_2(H_2O)_6\{H_4Mo_8O_{28}\}]\cdot 4H_2O$ (**1a**) and $[Co(ox)(NH_3)_4]_2[Al(mal)_2(H_2O)_2]\cdot Hmal\cdot 2H_2O$ (**1b**), were also isolated. Compounds $[Co(NH_3)_6][Al(mal)_2(H_2O)_2](NO_3)_2\cdot H_2O$ (**9**) and $[Co(en)_3]_2[Mo_8O_{26}(H_2O)_2]Cl_2\cdot 6H_2O$ (**10**) were the only products obtained from reactions involving Al^{3+} as the heteroatom and complex cations $[Co(NH_3)_6]^{3+}$ or $[Co(en)_3]^{3+}$. All compounds were prepared by hydrothermal synthesis and the mechanochemical method followed by vapour-assisted ageing. The reactions between sodium molybdate and $[Co(ox)(NH_3)_4]NO_3\cdot H_2O$ in the presence of $AlCl_3$ or GeO_2 and malonic acid were monitored *in situ* by Raman spectroscopy. The initial transformation involves a remarkably fast reaction between sodium molybdate and malonic acid, generating new species that subsequently reacted with other mixture components. The photocatalytic activities of compounds **1**, **2**, **4** and **5** in the degradation of the safranin T dye under visible light irradiation, both with and without hydrogen peroxide, were also examined. Compounds **4** and **5** exhibit the highest activities. To investigate the mechanisms driving the crystallization process, we monitored the transformation kinetics of amorphous intermediates into the final crystalline products within an aqueous slurry at room temperature. We employed *ex situ* powder X-ray diffraction (PXRD), a technique allowing real-time observation of structural changes as they occur. The resulting PXRD data, which generated complex, multi-dimensional datasets (data tensors), were analyzed using the 2nd-order tensor decomposition method, principal component analysis (PCA).

Received 23rd December 2025,
Accepted 20th January 2026

DOI: 10.1039/d5dt03064a

rsc.li/dalton

Introduction

Polyoxometalates (POMs) represent a large and structurally diverse class of metal-oxo clusters characterized by their rich structural topology and wide range of chemical and physical properties. A significant subclass of POMs comprises polyoxomolybdates (POMos), anionic molybdenum oxoclusters formed through the condensation of $\{MoO_4\}$ units. POMos containing exclusively molybdenum centres are classified as isopolyoxomolybdates, $[Mo_mO_y]$, whereas those incorporating an additional p-, d- or f-block metal heteroatom (X) are known as heteropolyoxomolybdates $[X_xMo_mO_y]$. The versatility in terms of their size, structure and redox activity makes them attractive candidates for numerous applications, including homogeneous and heterogeneous catalysis, biomedicine, and materials sciences.[1–10] The self-assembly of the molybdate ion, $[MoO_4]^{2-}$ and its transformation into higher-nuclearity species, as well as their crystallization into ionic POMo structures are governed primarily by a combination of hydrogen

[a]*Department of Chemistry, Faculty of Science, University of Zagreb, Horvatovac 102a, Zagreb, Croatia. E-mail: dkuzman@chem.pmf.hr, marina@chem.pmf.hr*
[b]*Department of Chemistry and Biochemistry, School of Medicine, University of Zagreb, Šalata 3, Zagreb, Croatia*
[c]*Ruđer Bošković Institute, Division of Materials Chemistry, Bijenička 54, 10000 Zagreb, Croatia*
[d]*Ruđer Bošković Institute, Division of Physical Chemistry, Bijenička 54, 10000 Zagreb, Croatia*

bonding and electrostatic interactions. Complex cations have proven to be exceptionally useful in POMo synthesis: beyond their role in charge balancing, they participate in supramolecular interactions that guide the condensation of $\{Mo_mO_y\}$ units, either by forming labile coordination complexes or through hydrogen bonding with reaction intermediates. These interactions contribute to templating and stabilization of polyoxomolybdate frameworks and influence their reactivity, structural diversity, and supramolecular organization. In recent years, research on polyoxomolybdates has shifted from focusing solely on their structural characterization to exploring their practical applications, such as photocatalysts for dye decomposition and wastewater treatment.[11–15] Photocatalytic degradation is considered a preferred, cleaner, and greener technology for removing toxic organic or inorganic pollutants from water.[16] In this process, the catalyst acts as a powerful oxidant, converting most of the organic contaminants into carbon dioxide and water when irradiated with light of an appropriate wavelength.[17–19] Besides their facile photoexcitation under near-visible or UV light, POMos offer advantages as both homogeneous or heterogeneous photocatalysts.

POMs display interesting redox activity and can undergo photoredox reactions to catalyse both oxidation and reduction of a wide variety of substrate molecules. The structure of POMs remains intact during the photoredox process, which is essential for their catalytic role. Due to the large number and types of metal centres, POMs can undergo multi-electron redox reactions, making them attractive candidates for multi-step photoredox systems. Re-oxidation of the reduced species is often achievable with molecular oxygen or hydrogen peroxide without degradation of the cluster compounds.[20,21]

This work is a continuation of our previous research on the influence of the synthetic route on the reactivity of the tris (ethylenediamine)cobalt(III), hexaamminecobalt(III) bis(ethylenediamine)oxalatocobalt(III), or tetraammineoxalatocobalt(III) cation and the molybdate anion in the presence of succinic and malonic acids.[22–26]

Herein, we explored the influence of the addition of heteroions Al^{3+}, Si^{4+}, Ge^{4+} and Te^{6+}, as well as malonic acid, on the self-assembly process of (hetero)polyoxoanions (Scheme 1). We also investigated the photocatalytic properties of selected hetropolyoxomolybdates, including two Keggin-type and two Anderson-type POMos. In addition, the kinetics of transformation of the amorphous intermediate into the final crystalline form in aqueous slurry at room temperature were studied by *ex situ* powder X-ray diffraction (PXRD) and Raman spectroscopy.

Results and discussion

Synthetic procedures

The development of synthetic methods, as well as improved detection methods (particularly in *in situ* approaches), has enabled a better understanding of and given more insight into pH-influenced self-assembly processes of polyoxomolybdates. Our previous investigations[19–21] have shown that the pH value of the solution and the choice of the complex cation as the counter ion are not quite independent. These studies focused on how the synthetic method, solution pH, the choice of the complex cation, and the presence of the mono- or dicarboxylic acid affect the formation of polyoxomoybdates and polyoxovanadates.[19–21]

In this study, we aimed to explore the influence of the complex cations $[Co(C_2O_4)(NH_3)_4]^+$, $[Co(NH_3)_6]^{3+}$, $[Co(C_2O_4)(en)_2]^+$ and $[Co(en)_3]^{3+}$ on the formation of heteropolyoxomolybdate species under hydrothermal or solid-state conditions. Sodium molybdate was used as the molybdenum precursor, while $AlCl_3{\cdot}6H_2O$, Na_2SiO_3, GeO_2 and H_2TeO_6 served as the sources of heteroatoms. The final products obtained by mechanochemically accelerated vapor-assisted aging are identical to those isolated by the hydrothermal method, yielding heteropolyoxometalates of the Anderson type (**1–3**) and Keggin-type (**4–7**), as well as coordination polymer **8** (Scheme 1). However, solid-state reactions enabled the iso-

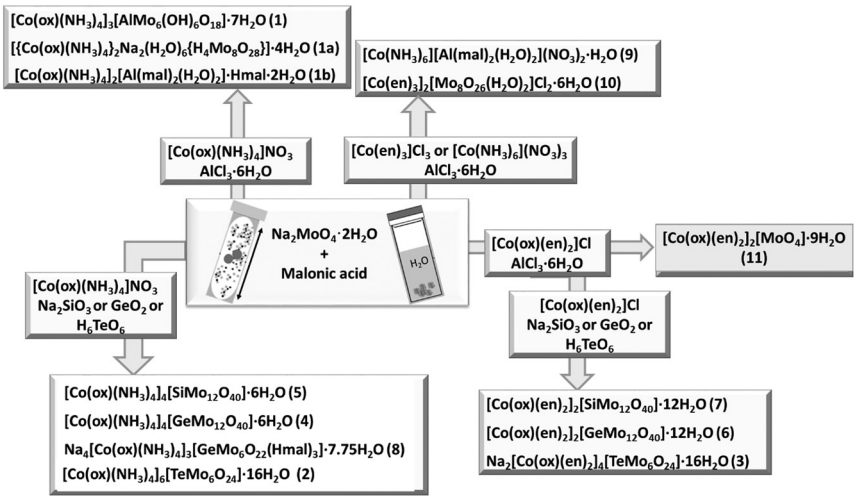

Scheme 1 Products obtained in reactions of $Na_2MoO_4{\cdot}2H_2O$, malonic acid, Co(III) complex cations and Al^{3+}, Si^{4+}, Ge^{4+} and Te^{6+} ions.

lation and characterization of two reaction intermediates, namely $[\{Co(ox)(NH_3)_4\}_2Na_2(H_2O)_6\{H_4Mo_8O_{28}\}]\cdot 4H_2O$ (**1a**) and $[Co(ox)(NH_3)_4]_2[Al(mal)_2(H_2O)_2]\cdot Hmal\cdot 2H_2O$ (**1b**), obtained from the reaction system containing the molybdate ion, malonic acid, aluminium(III) and tetraammineoxalatocobalt(III) cations.

In reactions performed with $[Co(en)_3]Cl_3$ or $[Co(NH_3)_6](NO_3)_3$, we were able to isolate products exclusively when aluminium was used as the heteroatom. The reaction carried out in the presence of tris(ethylenediamine)cobalt(III) yields only octamolybdate $[Co(en)_3]_2[Mo_8O_{26}(H_2O)_2]Cl_2\cdot 6H_2O$ (**10**) as the final product, whereas with hexaamminecobalt(III) it resulted in the formation of the Al(III) complex $[Co(NH_3)_6][Al(mal)_2(H_2O)_2](NO_3)_2\cdot H_2O$ (**9**).

We also attempted to isolate heteropolyvanadates in reactions of sodium vanadate with the above-mentioned salts, but all reactions, regardless of the added complex cation or synthetic method used, resulted in decavanadates $[H_2V_{10}O_{28}]^{4-}$ or $[V_{10}O_{28}]^{6-}$.[20] We can assume that these are the least soluble species under the given reaction conditions.

Thermal, spectroscopic, catalytic and Raman studies

Thermogravimetric and powder diffraction studies were carried out on polyoxomolybdates **1–4** and **6–10**.

The thermal study of all compounds was carried out in an oxygen atmosphere and in a temperature interval 25–600 °C (Table S1 and Fig. S1–S11). The main endothermic processes, dehydration and decomposition of the anhydrous part of the examined compounds, were observed, in agreement with other investigations and literature data.[27] We compared thermogravimetric data for products obtained in both synthetic paths and the data confirmed that the final products of all reactions were the same. The first endotherm stage obtained in the range of 34–365 °C (for **1**), 42–193 °C (for **1a**), 35–189 °C (for **2**), 30–198 °C (for **3**), 32–217 °C (for **6**), 29–214 °C (for **7**), 31–137 °C (for **8**), 343–94 °C (for **9**) and 36–140 °C (for **10**) is associated with the loss of water molecules. The second weight loss (in the range from 138 °C to 515 °C) is assigned to the continuous degradation of polyoxometalates and occurs in one stage for compounds **1a**, **3**, **6**, **7**, **8** and **9**. For compounds **2** and **10** degradation of polyoxometalates occurs in two stages: first in the range of 191–348 °C for **2** and 157–314 °C for **10**; and second in the range of 350–428 °C for **2** and 316–358 °C for **10**. The degradation of compounds **1b** and **4** was obtained in one step. The residual solids were mixed oxides MoO_3 + Co_xO_y + MO_y (M = Si, Ge, Te) or Co_xO_y + M_xO_y (M = Al, Na).

The IR spectra of the prepared compounds **1–11** were analyzed in detail and correlated with structural information obtained by X-ray analysis, as well as data reported in the literature.[28–35] In the IR spectra of all compounds, except for **1b** and **8**, the strong bands between 979 and 856 cm^{-1} were assigned to the stretching vibrations of terminal Mo–O bonds. Very strong bands observed in the regions 886–810 cm^{-1} and 575–722 cm^{-1} were assigned to the Mo–O stretching within the Mo–O–Mo bridges. Broad, medium-intensity bands in the range 3138–3285 cm^{-1} confirmed the existence of the O–H···O hydrogen bonds. The bands in the region of 3530–3472 cm^{-1} were ascribed to the N–H and O–H bond vibrations. In the spectra of compounds **1**, **1a**, **1b**, **2–9**, and **11**, strong bands at 1724–1677 cm^{-1} and 1440–1160 cm^{-1} were assigned to the asymmetric and symmetric stretching vibrations of C–O and C–C bonds in $C_2O_4^{2-}$ and $H_3C_3O_4^-$ (present in **1b**, **8**, **9**) ions (Table S2 and Fig. S12–S22).

In our studies on the reaction mechanism or catalytic activities, we selected heteropolyoxomolybdates containing the $[Co(ox)(NH_3)_4]^+$ cation, since all heteroatoms used successfully yielded the corresponding polyoxo species. Therefore, in an attempt to establish the reaction mechanism of heteropolyoxomolybdate formation, we examined two model reactions by Raman spectroscopy *in situ*:

- reaction of sodium molybdate with $AlCl_3\cdot 6H_2O$ in the presence of $[Co(ox)(NH_3)_4]^+$ and malonic acid,
- reaction of sodium molybdate with GeO_2 in the presence of $[Co(ox)(NH_3)_4]^+$ and malonic acid.

The main obstacle that we encountered during *in situ* reaction monitoring was sticky reaction mixtures, which exhibited a strong tendency to adhere to reaction vessel walls causing improper mixing and even complete loss of Raman signal. Nevertheless, we succeeded in observing that sodium molybdate, a common precursor in both reactions, reacted remarkably fast with malonic acid. This led to the formation of a species that had its strongest band very close to the strongest band of sodium molybdate at about 891 cm^{-1}. This indicated that, for the reaction mixture, the first transformation involved the reaction of sodium molybdate and malonic acid and the newly formed species reacted with the cobalt complex (Fig. 1 and 2). We attempted to characterize this new species by powder X-ray diffraction but were not successful. The only other species that could be tracked in the Raman spectra was the cobalt complex. Altogether, these two species disappeared suddenly after *ca.* half an hour of milling, providing the milling product. While sudden reactions are known in mechanochemistry, in this case, it cannot be excluded that the abrupt change in Raman spectra was due to the rheological properties of the reaction mixture, which may have resulted in redistribution of the materials inside the reaction vessel.

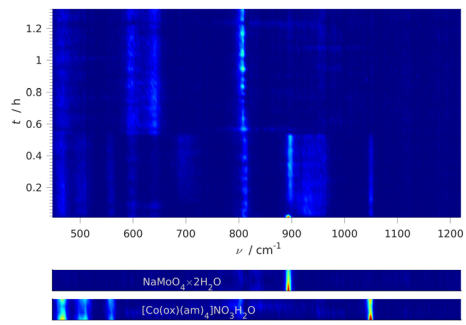

Fig. 1 Time-resolved *in situ* Raman spectra of the reaction of $Na_2MoO_4\cdot H_2O$, malonic acid and $[Co(ox)(NH_3)_4]NO_3\cdot H_2O$. The Raman spectra of reactants are shown below the reaction spectra. Malonic acid did not provide any significant Raman scattering.

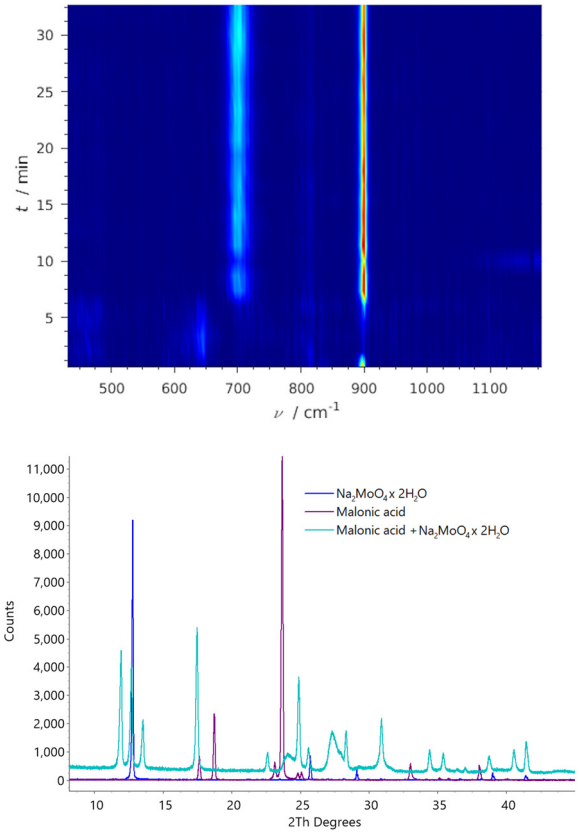

Fig. 2 (Top) Time resolved Raman spectra for milling of sodium molybdate and malonic acid. (Bottom) Powder X-ray diffraction patterns of the reactants and the product showing the formation of new crystalline species.

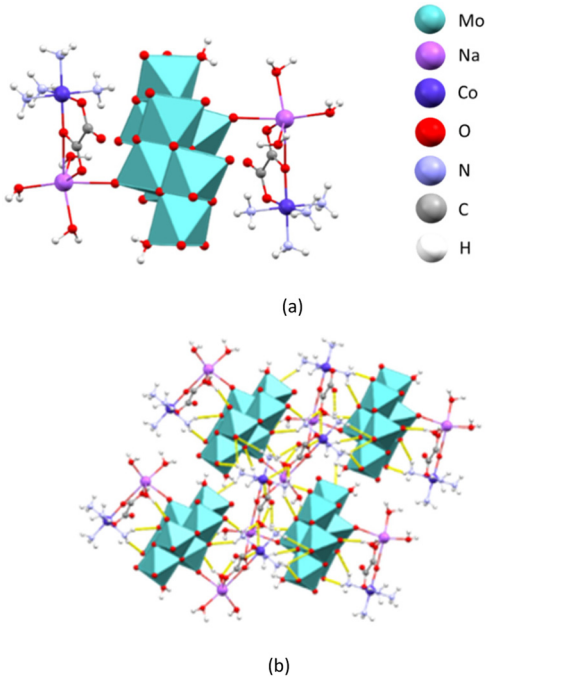

Fig. 3 Structure of **1a**: (a) coordination environment of metal ions; (b) a hydrogen-bonded layer of anions and cations perpendicular to the crystallographic *c*-axis.

Structural investigations

Iso(poly)oxomolybdate species $[\{Co(ox)(NH_3)_4\}_2Na_2(H_2O)_6\{H_4Mo_8O_{28}\}]\cdot 4H_2O$ (**1a**), $[Co(en)_3]_2[Mo_8O_{26}(H_2O)_2]Cl_2\cdot 6H_2O$ (**10**), and $[Co(ox)(en)_2]_2[MoO_4]\cdot 9H_2O$ (**11**) have been prepared by mechanochemical reactions and characterized. Compound **1a** crystalizes in the *P*21/*n* space group (crystallographic data given in SI Table S3) and its asymmetric unit contains one half of a γ-octamolybdate anion[36,37] with two terminal oxygen atoms substituted by water molecules, a $[Co(ox)(NH_3)_4]^+$ cation, a sodium cation and five water molecules. The sodium cation is coordinated by a terminal oxo atom of the molybdate and two oxygen atoms from the oxalate ligand of the complex cation, thus bridging the polyanion and the cobalt(III) cation (Fig. 3a). Three additional water molecules coordinate the sodium atom, making the coordination number of sodium seven. There is an extensive hydrogen bond network present in **1a**, which interconnects anions and cations into a three-dimensional supramolecular framework (Fig. 3b). Ammine ligands of the complex cation are hydrogen bond donors and form hydrogen bonds with the oxygen atoms of the anion and the oxygen atoms of the neighbouring oxalato ligands (SI Table S6).

In **10** the structure of the asymmetric unit is made up of two symmetrically independent halves of the γ-octamolybdate anion,[25,26] two $[Co(ox)(en)_2]^{3+}$ cations and two charge compensating chloride anions. Compound **10** crystalizes in the $P\bar{1}$ space group (crystallographic data given in SI Table S5). Unlike the anions in **1a** that are coordinated by two sodium atoms, the anions in **10** form supramolecular chains by hydrogen bonding *via* coordinated water molecules (Fig. 4a). The anionic chains are further interconnected by hydrogen bonds formed by ethylenediamine groups of the cations and oxo ligands of the anion (SI Table S7) into a three-dimensional framework in such a way that leaves voids containing water molecules (Fig. 4b). Isolated compound **11** has been previously reported in the literature.[38]

Two complex aluminium(III) salts with different cobalt(III) cations have been isolated and characterized, namely $[Co(ox)(NH_3)_4]_2[Al(mal)_2(H_2O)_2]\cdot Hmal\cdot 2H_2O$ (**1b**) and $[Co(NH_3)_6][Al(mal)_2(H_2O)_2](NO_3)_2\cdot H_2O$ (**9**). Compound **1b** crystalizes in the $P2_1/c$ space group, while **9** crystalizes in the *Cc* space group (crystallographic data given in SI Table S3 for **1b** and Table S5 for **9**). Both salts contain the $[Al(mal)_2(H_2O)_2]^-$ anion, where two malonate anions coordinate the aluminium ion in a bidentate chelating fashion in the equatorial plane, while two water molecules take up the axial positions (Fig. 5a). The geometry of the anion is in accordance with the structures previously reported in the literature.[39] Additional hydrogen malonate in **1b** and two nitrates in the unit cell of **9** compensate for the net positive charge of the complex species. There is considerable hydrogen bonding in both compounds, with ammine groups and water molecules serving as hydrogen bond donors and oxygen atoms of oxalate ligands (in **1b**) and

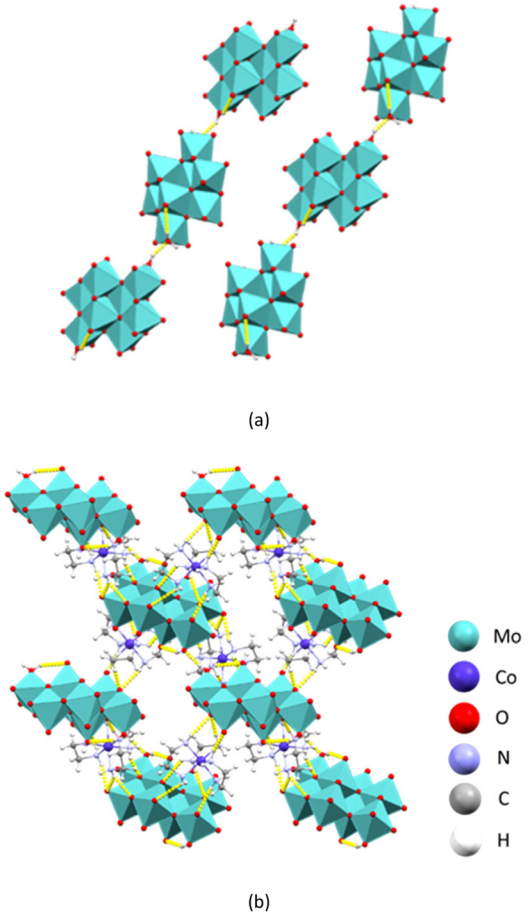

Fig. 4 Structure of **10**: (a) supramolecular chains comprising hydrogen bonded anions; (b) a hydrogen-bonded layer of anions and cations perpendicular to the crystallographic *a*-axis.

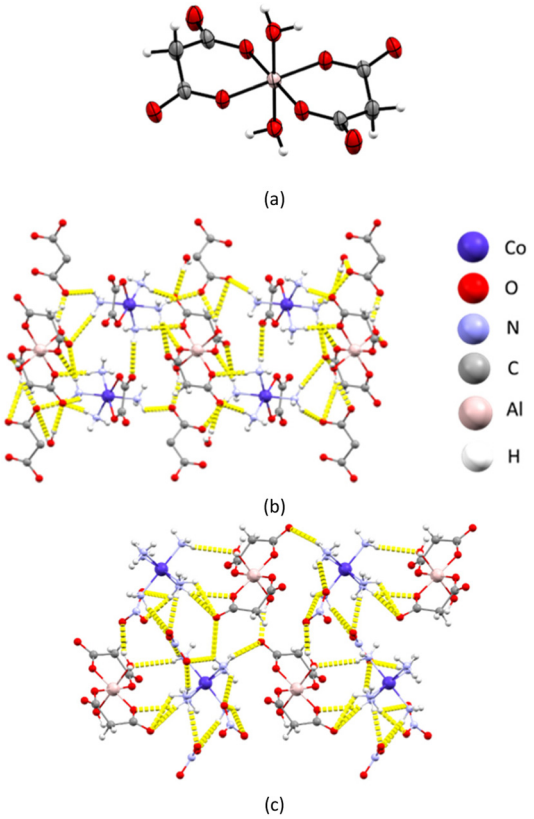

Fig. 5 (a) $[Al(mal)_2(H_2O)_2]^-$ anion present in both **1b** and **9**; (b) a hydrogen-bonded layer of anions and cations perpendicular to the crystallographic *b*-axis in **1b**; (c) hydrogen-bonded layer of anions and cations perpendicular to the crystallographic *a*-axis in **9**.

water molecules being the acceptors (list of hydrogen bonds given in SI Tables S8 and S9). Anions and cations form a three-dimensional supramolecular framework (Fig. 5b and c).

Three Anderson-type heteropolyoxomolybdates with aluminium and tellurium have been isolated. The compound $[Co(ox)(NH_3)_4]_3[AlMo_6(OH)_6O_{18}]\cdot 7H_2O$ (**1**) is found to crystallize in the space group *C*2/*c*, the compound $[Co(ox)(NH_3)_4]_6[TeMo_6O_{24}]\cdot 16H_2O$ (**2**) in $P\bar{1}$ and the compound $Na_2[Co(ox)(en)_2]_4[TeMo_6O_{24}]\cdot 16H_2O$ (**3**) in the *C*2/*c* space group (crystallographic data given in SI Table S3 for **1** and **2**, and Table S4 for **3**). While all of the mentioned compounds contain Anderson-type hetero POMos, which are structurally similar, they differ in their protonation states. The aluminium POMo contains six protonated bridging oxygen atoms unlike the tellurium Anderson anion, which is not protonated. The two heteroPOMo anions also differ in the oxidation state of the hetero atom, *i.e.* aluminium being in the +3 and tellurium in the +6 oxidation state. The structure of the POMo anions is shown in Fig. 6a and b and is in accordance with the ones previously reported in the literature.[40] The anions and complex cations in the three compounds participate in numerous hydrogen bonds that form three-dimensional supramolecular frameworks (Fig. 4c and d). The list of hydrogen bonds is given in SI Tables S7–S9.

Four Keggin-type heteropolyoxomolybdate compounds have been isolated, namely two with the $[Co(ox)(NH_3)_4]^+$ cation and two with the $[Co(ox)(en)_2]^+$ cation. Compounds $[Co(ox)(NH_3)_4]_4[GeMo_{12}O_{40}]\cdot 6H_2O$ (**4**) and $[Co(ox)(NH_3)_4]_4[SiMo_{12}O_{40}]\cdot 6H_2O$ (**5**) are isostructural, and **5** has been previously described and published in the literature.[19] $[Co(ox)(en)_2]_4[GeMo_{12}O_{40}]\cdot 12H_2O$ (**6**) and $[Co(ox)(en)_2]_4[SiMo_{12}O_{40}]\cdot 12H_2O$ (**7**) are isostructural as well. They crystalize in the *P*21/*n* space group (crystallographic data given in SI Table S4). The asymmetric unit of **6** and **7** comprises one half of the Keggin type hetero-POMo anion and two $[Co(ox)(en)_2]^+$ cations. The dimethylamine ligands of the complex cations act as hydrogen bond donors with oxygen atoms of the anion being the acceptors of the bonds (Fig. 7b). Bond lengths are given in SI Table S12 for **6** and Table S13 for **7**. The hydrogen bond network formed by anions and cations leaves voids that contain solvent molecules (Fig. 7c).

A mechanochemical reaction of sodium molybdate, germanium(IV) oxide, malonic acid and the $[Co(ox)(NH_3)_4]^+$ cation yielded a novel hetero-POMo coordination polymer $Na_4[Co(ox)(NH_3)_4]_3[GeMo_6O_{22}(Hmal)_3]\cdot 7.75H_2O$ (**8**). Compound **8** crystallizes in the $P\bar{1}$ space group (crystallographic data given in SI Table S3). The anion is built of six $\{MoO_6\}$ octahedra con-

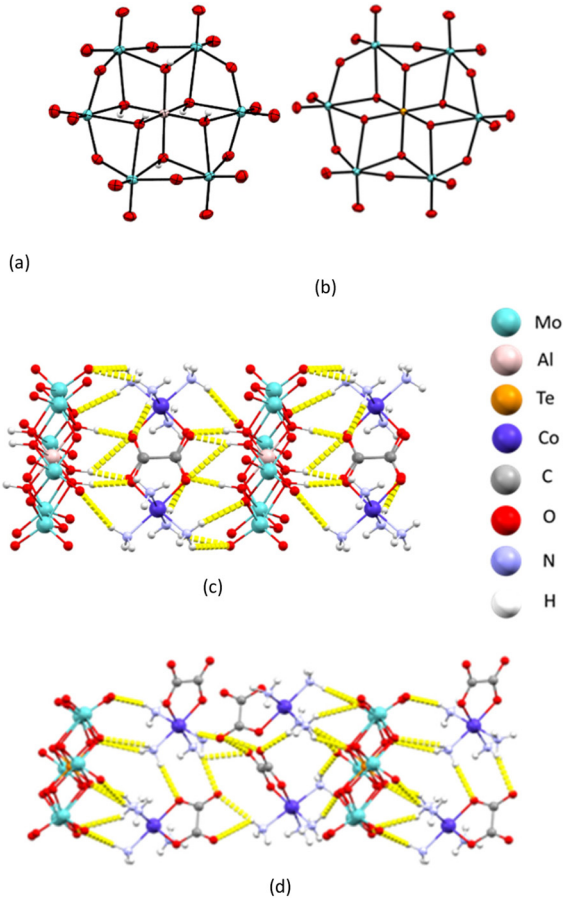

Fig. 6 (a) $[AlMo_6(OH)_6O_{18}]^{3-}$ anion present in **1**; (b) $[TeMo_6O_{24}]^{6-}$ anion present in **2**; (c) hydrogen-bonded layer of anions and cations perpendicular to the crystallographic *b*-axis in **1**; (d) hydrogen-bonded layer of anions and cations perpendicular to the crystallographic *b*-axis in **2**.

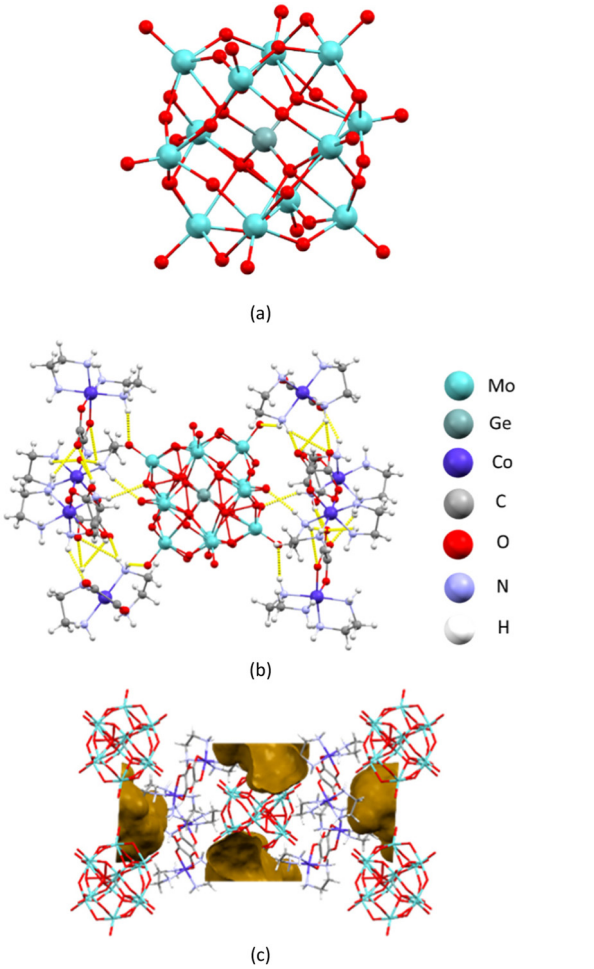

Fig. 7 (a) $[GeMo_{12}O_{40}]^{4-}$ anion present in **6**; (b) hydrogen bond network of the $[GeMo_{12}O_{40}]^{4-}$ anion and neighbouring cations; (c) porous structure of **6**.

nected by edges or vertices with two neighbouring octahedra being bridged by a hydrogen malonate, and a $\{GeO_4\}$ tetrahedron situated in the centre of the molybdate ring (Fig. 8a). This is, to our knowledge, the first hybrid organic–inorganic hetero-POMo of this type. The structure of the anion is similar to a part of the Keggin type molybdate (Fig. 9), which could indicate that malonic acid plays a crucial role in the formation of POMos. Sodium atoms coordinate the oxo ligands of the anion, bridging them with each other and with neighbouring cobalt(III) cations *via* their oxalate ligands, forming an extensive three-dimensional coordination framework (Fig. 8b).

Our investigations also aimed to characterize the transformation of an amorphous precipitate into crystalline products **1**, **2**, **4**, and **5** during room temperature aging (Fig. 10 and 11). We monitored this transformation *ex situ* using the powder X-ray diffraction method (PXRD). The representative PXRD pattern for compound **5** is given in Fig. 12, while for compounds **1**, **2**, and **4** in Fig. S27–S29. PXRD patterns of all compounds are given in Fig. S30.

The PXRD data revealed that the amorphous solid rapidly converted to the final crystalline product after an initial induction period, during which no significant changes were observed. This supports the hypothesis that nucleation of the crystalline phase is the rate-determining step; once nuclei form, crystal growth proceeds quickly.

The induction time and overall transformation time varied considerably among the different compounds (from 20 to 60 hours for the presented compounds, Fig. 10–13). Principal component analysis of the PXRD data (Table 1) demonstrated that the reaction progress could be effectively modelled using only the first principal component (PC1).[41] PC1 in each case explained over 55% of the total variance (compounds **1**, **2**, **4**, and **5**) and accurately tracked the reaction's progression and completion. The first three principal components cumulatively explained over 90% of the variance. Validation of the PCA-derived reaction profiles confirmed that reactions were completed within the predicted timeframes: approximately 50 hours for compounds **1** and approx. 30 hours for other compounds. Representative profiles are given in Fig. 13 and 14.

The photocatalytic performance of the heteropolyoxomolybdates, including two of the Anderson-type compounds (**1** and

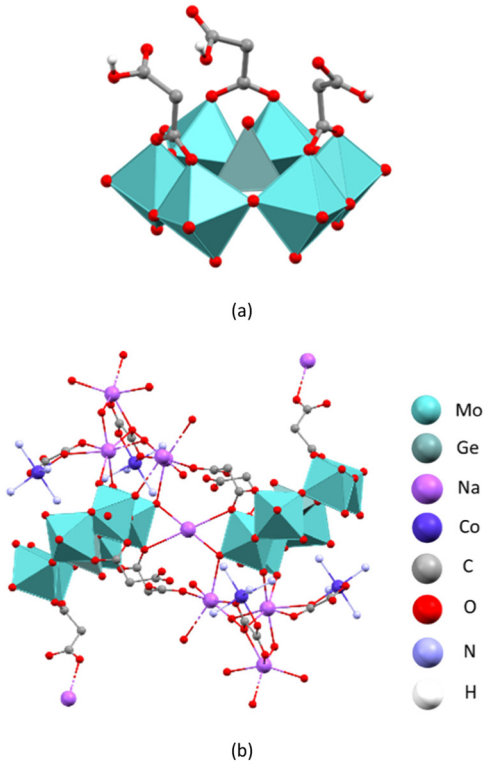

Fig. 8 Structure of **8**: (a) the $[GeMo_6O_{22}(Hmal)_3]^{7-}$ anion; (b) a fragment of the coordination polymer layer perpendicular to the crystallographic *b* axis.

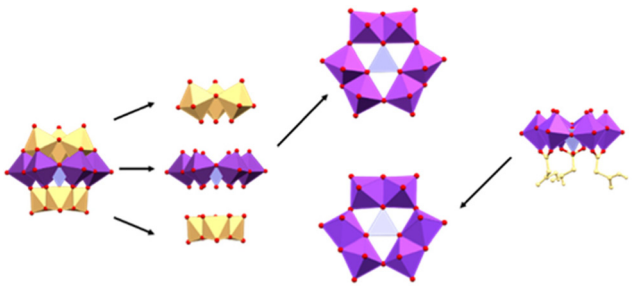

Fig. 9 Similarities between the Keggin type heteroPOMo $[GeMo_{12}O_{40}]^{4-}$ (**4**) (left) and the $[GeMo_6O_{22}(Hmal)_3]^{7-}$ anion present in **8** (right).

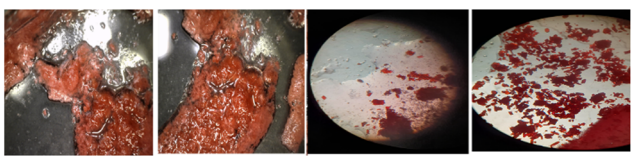

Fig. 10 Grained mixture of **1** after 0, 24, 72 and 96 h in 100% humidity at R.T.

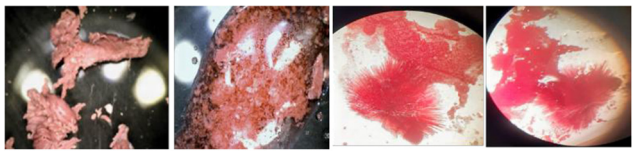

Fig. 11 Grained mixture of **5** after 0, 24, 72 and 96 h in 100% humidity at R.T.

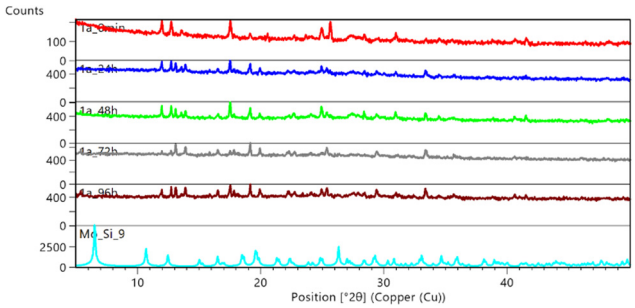

Fig. 12 *Ex situ* PXRD monitoring of the transformation of the amorphous precipitate of **5** to the crystallite.

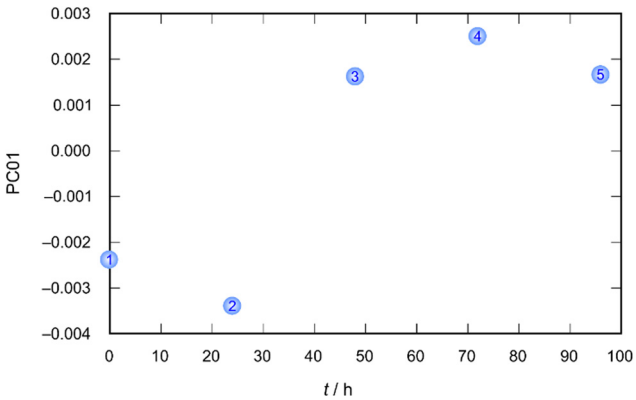

Fig. 13 Reaction profile represented by the time dependence of PC1 scores calculated for a set of PXRD data collected for complex compounds **1**.

2) and four of the Keggin type compounds (**4**, **5**, **6** and **7**), was evaluated using a safranin T dye solution at room temperature. These compounds were selected to enable a comparative analysis and to investigate the effect of anion composition and structure on the observed properties.

The experiments were conducted (a) with heteropolyoxomolybdates under visible light irradiation (420–650 nm) and (b) in the case where heteropolyoxomolybdates showed no catalytic activity after irradiation, in combination with H_2O_2.

The absorption experiments were performed as follows: 20 mg of compound **1**, **2**, **4**, **5**, **6** or **7** was added to 20 mL of 0.035 mol dm^{-3} aqueous safranin solution. Solutions were kept in the dark. At selected time intervals, the clear supernatant obtained after centrifugation was transferred to a quartz cuvette to record the UV-Vis spectra in the range of 400–600 nm. In the case of compounds **1** and **2** no catalytic activity was observed so the following experiments were performed: 20 mg of compound **1** or **2** was added to 20 mL of a

Table 1 Total variance represented by the first principal components calculated for a set of PXRD data collected through transformations

	1		2		4		5	
Component	Individual	Cumulative	Individual	Cumulative	Individual	Cumulative	Individual	Cumulative
PC1	87.54	87.54	70.08	70.08	58.85	58.85	55.75	55.75
PC2	6.50	94.04	23.01	93.09	21.68	80.53	22.77	78.52
PC3	4.52	98.57	4.15	97.25	12.36	92.90	11.43	89.96

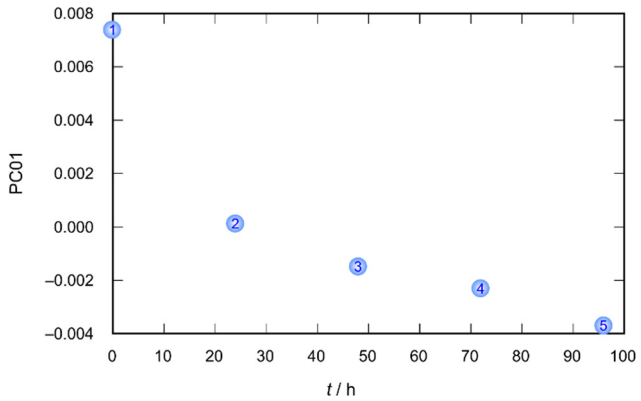

Fig. 14 Reaction profile represented by the time dependence of PC1 scores calculated for a set of PXRD data collected for compound **5**.

0.035 mol dm^{-3} aqueous safranin solution, together with 0.5 mL of 30% H_2O_2 solution in a glass bottle, and irradiated under UV for 180 min. During the experiment, the mixtures were continuously stirred. At selected time intervals, the sample mixtures were taken out from the reactor, centrifuged and analyzed. As shown in Fig. 15, compounds **4**, **5**, **6** and **7** catalyze the decomposition of the dye without the presence of hydrogen peroxide.

All of the listed compounds are of the Keggin type which indicates that the reaction catalytic center is most likely heteropolyoxomolybdate. Although the reaction rate constants among Keggin types vary from compound to compound by a few orders of magnitude, the exact reason for that is hard to pinpoint considering different crystal sizes of the prepared crystals.

An attempt to perform a catalytic test with pulverized compound **5** led to a significant increase in catalytic activity that it made it very hard to calculate reaction rates (more than 85% dye degradation in 30 min) (Fig. S26g). Anderson type compounds showed no catalytic activity of their own but in combination with hydrogen peroxide they had co-catalytic effect that leads to complete degradation of the dye (Fig. S26). Since a UV filter was used, peroxide degradation without the addition of heteropolyoxomolybdate was slow and therefore dye degradation was only partial. The addition of **1** and **2** facilitated the generation of OH radicals without exposure to UV light (Fig. 16).

Decomposition mechanisms were further confirmed using radical scavengers: benzoquinone (BQ, for $O_2^{\bullet}$ radicals), isopropyl alcohol (IPA, for $OH^{\bullet-}$ radicals) and ethylenediaminetetraacetic acid (EDTA, h^+ holes). The addition of IPA to the compounds **1** and **2** catalytic test inhibited decomposition, while the other two scavengers only showed a slight decrease in catalytic activity compared to the reference reaction without a scavenger. In the case of **4**, **5**, **6** and **7** additions of BQ and EDTA, there is no significant decrease in catalytic activity, which indi-

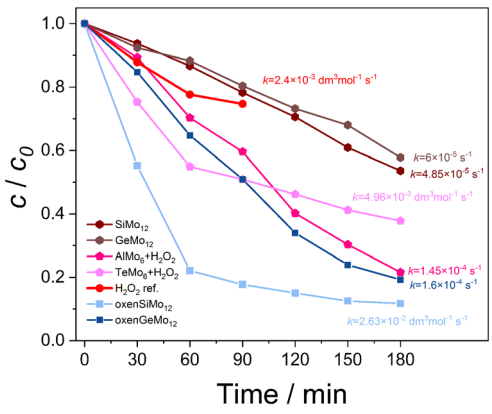

Fig. 15 $[Co(ox)(NH_3)_4]_4[GeMo_{12}O_{40}]\cdot 6H_2O$ (**4**), $[Co(ox)(NH_3)_4]_4[SiMo_{12}O_{40}]\cdot 6H_2O$ (**5**), $[Co(ox)(en)_2]_4[GeMo_{12}O_{40}]\cdot 12H_2O$ (**6**) and $[Co(ox)(en)_2]_4[SiMo_{12}O_{40}]\cdot 12H_2O$ (**7**) catalyze the decomposition of the dye without the presence of hydrogen peroxide.

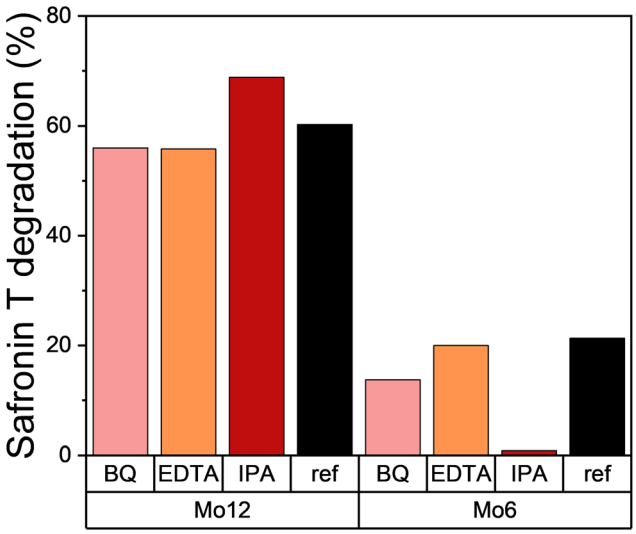

Fig. 16 Reaction of Anderson and Keggin POMs with benzoquinone (BQ). EDTA = ethylenediaminetetraacetic acid, IPA = isopropyl alcohol.

cates that the reaction mechanism is most likely based on reduction of molybdenum(VI) to molybdenum(V) or some combination of $O_2^{\bullet}$ radicals and holes.

Comparison of the PXRD patterns before and after the catalytic experiments for compounds **1**, **2**, **4**, **5**, **6** and **7** is given in Fig. S31.

Experimental

Materials and methods

The starting cobalt(III) complex salts, tris(ethylenediamine) cobalt(III) chloride ($[Co(en)_3]Cl_3$), bis(ethylenediamine)oxalatocobalt(III) chloride monohydrate ($[Co(C_2O_4)(en)_2]Cl{\cdot}H_2O$), hexaamminecobalt(III) nitrate ($[Co(NH_3)_6](NO_3)_3$) and tetraammineoxalatocobalt(III) nitrate monohydrate ($[Co(C_2O_4)(NH_3)_4]NO_3{\cdot}H_2O$), were prepared according to the previously reported procedures.[42] Sodium molybdate dihydrate ($Na_2MoO_4{\cdot}2H_2O$), sodium metasilicate (Na_2SiO_3), aluminium chloride hexahydrate ($AlCl_3{\cdot}6H_2O$), germanium(IV) oxide (GeO_2), telluric acid (H_6TeO_6) and malonic acid ($HOOCCH_2COOH$; H_2mal) were commercially available; reagent-grade chemicals were used as received without further purification. A Retsch MM200 grinder mill operating at 25 Hz frequency was used for the synthesis. Elemental analyses were carried out with a Perkin-Elmer Series II 2400 CHNS/O analyser. Infrared spectra were recorded on a PerkinElmer Spectrum RXI FTIR spectrometer from samples dispersed in KBr pellets (4000–400 cm^{-1} range). Chemical analyses were provided by the Analytical Services Laboratory of the Ruđer Bokšović Institute, Zagreb and by the Analytical Services Laboratory of the University of Zagreb Faculty of Science and Faculty of Forestry. The crystal structures were determined by single-crystal and powder X-ray diffraction.

Single-crystal and powder X-ray diffraction experiments

Powder patterns were collected at room temperature in the range from 5 to 50° (2θ) with a step size of 0.043 and 7.14 s per step. The data were collected and visualized by using the Malvern Panalytical High Score Software Suite.[43] Single-crystal X-ray diffraction data of **1–11** were collected on an XtaLAB Synergy-SCCD diffractometer with CuKα (λ = 1.54184 Å) radiation at room temperature or at 170 K. Data reduction was performed using the CrysAlis software package.[44] Solution, refinement, and analysis of the structures were done using the programs integrated in the WinGX61 and OLEX262 systems. All structures were solved and refined with the SHELX program suite.[45] Structural refinement was performed on F^2 using all of the data. All hydrogen atoms were placed at the calculated positions and treated as riding on the parent atoms. Geometrical calculations were done using PLATON.[46] Drawings of the structures were prepared using PLATON and MERCURY programs.[47] Powder X-ray diffraction (PXRD) data were collected on a Malvern Panalytical Aeris powder diffractometer in the Bragg–Brentano geometry with the aPIXcel1D detector, using CuKα radiation (λ = 1.5406 Å). Samples were placed on a Si sample holder.

Catalytic experiments

The catalytic tests were performed by mixing 20 mg of ground sample with 20 mL of safranin T solution (c = 0.035 mol dm^{-3}) in a 100 mL glass at room temperature. The solution for catalysis was mixed using a magnetic stir bar at 550 rounds per minute. A Xenon light source of 300 W (MAX-303) with a 420–650 nm filter was used for irradiation. UV/vis measurements were performed using a UV-3600 (Shimadzu) in a 1 cm quartz cuvette. When hydrogen peroxide was used, 0.5 mL of 30% solution was added to the reaction mixture. Before UV/vis measurement, the catalyst was removed from the solution using a centrifuge.

Principal component analysis

Principal Component Analysis (PCA) was employed as a dimensionality reduction technique to analyze the PXRD data. PCA decomposes a data matrix X (with mean-centered columns) into a sum of rank-one matrices, effectively identifying the directions of maximum variance within the dataset. This analysis provides two key outputs: scores and loadings. Scores represent projections of the original PXRD spectra onto the principal component (PC) directions and can be used for classification or statistical analysis. Loadings, which are the eigenvectors of the data covariance matrix, represent the contribution of each variable (PXRD angle) to the variance captured by each PC. Importantly, the loadings retain the original intensity units of the PXRD spectra. The historical development of PCA traces back to Beltrami and Pearson,[48,49] with the term principal component coined by Hotelling.[50] The PCA was implemented using a NIPALS algorithm[51] within our own multivariate code, *moonee*.[52–54] Further details on PCA can be found in the recent literature.

Synthetic procedures

Liquid-assisted ball milling followed by vapour-assisted ageing

*General procedure for synthesis of compounds **1**, **1a**, **1b**, **2–11**.* A mixture of $Na_2MoO_4{\cdot}2H_2O$ (0.60 mmol, 145 mg), the corresponding Co(III) complex (0.30 mmol; 104 mg for $[Co(en)_3]Cl_3$, 96 mg for $[Co(C_2O_4)(en)_2]Cl{\cdot}H_2O$, 104 mg for $[Co(NH_3)_6](NO_3)_3$, or 89 mg for $[Co(C_2O_4)(NH_3)_4]NO_3{\cdot}H_2O$), malonic acid ($H_2mal$, 1.2 mmol, 125 mg), the appropriate heteroatom source (0.10 mmol; 12 mg for Na_2SiO_3, 24 mg for $AlCl_3{\cdot}6H_2O$, 10 mg for GeO_2, or 23 mg for H_6TeO_6) and acetone (10 μL) was placed in a 10 mL Teflon jar. For compounds **2** and **4** a mixture of $Na_2MoO_4{\cdot}2H_2O$ (0.26 mmol, 62 mg), $[Co(C_2O_4)(NH_3)_4]NO_3{\cdot}H_2O$ (0.26 mmol, 76 mg), malonic acid (0.26 mmol, 27 mg), and H_6TeO_6 (0.043 mmol, 9.9 mg) was used and for compound **4**, a mixture of $Na_2MoO_4{\cdot}2H_2O$ (0.52 mmol, 125 mg), $[Co(C_2O_4)(NH_3)_4]NO_3{\cdot}H_2O$ (0.17 mmol, 51 mg), malonic acid (1.2 mmol, 125 mg), and GeO_2 (0.043 mmol, 4.5 mg) was used, respectively. The reactants were milled for 30 min at a frequency of 25 Hz. The resulting reaction mixture was then exposed to 100% relative humidity at room temperature. The crystalline products were mechanically separated from the reaction mixture, washed with cold water, and dried in a desiccator.

1. $[Co(C_2O_4)(NH_3)_4]_3[AlMo_6(OH)_6O_{18}]\cdot 7H_2O$. Pink-red crystals of **1** were obtained after 2.5 weeks. Yield: 15.70 mg. Anal. calcd (%) for $C_6H_{56}N_{12}O_{43}AlCo_3Mo_6$: C 4.09, H 3.20, N 9.53, Al 1.53, Co 10.02, Mo 32.64. Found: C 4.15, H 3.11, N 9.48, Al 1.48, Co 9.95, Mo 32.23.

1a. $[\{Co(C_2O_4)(NH_3)_4\}_2Na_2(H_2O)_6\{H_4Mo_8O_{28}\}]\cdot 4H_2O$. Red crystals of **1a** were obtained after 1 week. Yield: 7.00 mg. Anal. calcd (%) for $C_4H_{48}N_8O_{46}Na_2Co_2Mo_8$: C 2.56, H 2.58, N 5.97, Na 2.45, Co 6.28, Mo 40.92. Found: C 2.72, H 2.75, N 6.06, Na 2.33, Co 6.11, Mo 40.71.

1b. $[Co(C_2O_4)(NH_3)_4]_2[Al(C_3H_2O_4)_2(H_2O)_2]\cdot C_3H_3O_4\cdot 2H_2O$. Pink crystals of **1b** were obtained after 2 weeks. Yield: 5.60 mg. Anal. calcd (%) for $C_{13}H_{39}N_8O_{24}AlCo_2$: C 18.67, H 4.70, N 13.40, Al 3.23, Co 14.09. Found: C 18.84, H 4.89, N 13.52, Al 3.09, Co 13.97.

2. $[Co(C_2O_4)(NH_3)_4]_6[TeMo_6O_{24}]\cdot 16H_2O$. Red crystals of **2** were obtained after one week. Yield: 5.00 mg. Anal. calcd (%) for $C_{12}H_{104}N_{24}O_{64}Co_6Mo_6Te$: C 5.41, H 3.93, N 12.61, Co 13.26, Mo 21.59, Te 4.79. Found: C 5.49, H 3.99, N 12.52, Co 12.95, Mo 21.05, Te 4.63.

3. $Na_2[Co(C_2O_4)(en)_2]_4[TeMo_6O_{24}]\cdot 16H_2O$. Red crystals of **3** were obtained after 2 months. Yield: 14.10 mg. Anal. calcd (%) for $C_{24}H_{96}N_{16}O_{56}Na_2Co_4Mo_6Te$: C 11.58, H 3.89, N 9.00, Na 1.85, Co 9.47, Mo 23.12, Te 5.12. Found: C 11.66, H 3.97, N 8.91, Na 1.74, Co 9.39, Mo 23.08, Te 5.07.

4. $[Co(C_2O_4)(NH_3)_4]_4[GeMo_{12}O_{40}]\cdot 6H_2O$. Red crystals of **4** were obtained after two months. Yield: 49.00 mg. Anal. calcd (%) for $C_8H_{60}N_{16}O_{62}Co_4GeMo_{12}$: C 3.39, H 2.14, N 7.91, Co 8.32, Ge 2.56, Mo 40.65. Found: C 3.46, H 2.20, N 7.79, Co 8.40, Ge 2.46, Mo 40.80.

5. $[Co(C_2O_4)(NH_3)_4]_4[SiMo_{12}O_{40}]\cdot 6H_2O$. Red crystals of **5** were obtained after 3 weeks. Yield: 12.45 mg. Anal. calcd (%) for $C_8H_{60}N_{16}O_{62}SiCo_4Mo_{12}$: C 3.45, H 2.17, N 8.04, Si 1.01, Co 8.46, Mo 41.30. Found: C 3.38, H 2.25, N 8.17, Si 0.95, Co 8.36, Mo 41.03.

6. $[Co(C_2O_4)(en)_2]_4[GeMo_{12}O_{40}]\cdot 12H_2O$. Red crystals of **6** were obtained after 3 months. Yield: 14.00 mg. Anal. calcd (%) for $C_{24}H_{88}N_{16}O_{68}Co_4GeMo_{12}$: C 9.15, H 2.82, N 7.12, Co 7.49, Ge 2.31, Mo 36.57. Found: C 9.21, H 2.91, N 7.07, Co 7.32, Ge 2.22, Mo 36.46.

7. $[Co(C_2O_4)(en)_2]_4[SiMo_{12}O_{40}]\cdot 12H_2O$. Red crystals of **7** were obtained after ten days. Yield: 10.80 mg. Anal. calcd (%) for $C_{24}H_{88}N_{16}O_{68}SiCo_4Mo_{12}$: C 9.29, H 2.86, N 7.22, Si 0.90, Co 7.59, Mo 37.09. Found: C 9.36, H 2.92, N 7.16, Si 0.83, Co 7.47, Mo 36.92.

8. $Na_4[Co(C_2O_4)(NH_3)_4]_3[GeMo_6O_{22}(C_3H_3O_4)_3]\cdot 7.75H_2O$. Pink crystals of **8** were obtained after 2 weeks. Yield: 11.20 mg. Anal. calcd (%) for $C_{15}H_{60.5}N_{12}O_{53.75}Na_4Co_3GeMo_6$: C 8.24, H 2.79, N 7.69, Na 4.21, Co 8.09, Ge 3.32, Mo 26.33. Found: C 8.31, H 2.71, N 7.78, Na 4.13, Co 7.98, Ge 3.19, Mo 26.12.

9. $[Co(NH_3)_6][Al(C_3H_2O_4)_2(H_2O)_2](NO_3)_2\cdot H_2O$. Yellow-orange crystals of **9** were obtained after 1.5 month. Yield: 10.65. Anal. calcd (%) for $C_6H_{28}N_8O_{17}AlCo$: C 12.64, H 4.95, N 19.65, Al 4.73, Co 10.33. Found: C 12.82, H 5.09, N 19.82, Al 4.58, Co 10.12.

10. $[Co(en)_3]_2[Mo_8O_{26}(H_2O)_2]Cl_2\cdot 6H_2O$. Orange crystals of **10** were obtained after 2 weeks. Yield: 15.50 mg. Anal. calcd (%) for $C_{12}H_{64}N_{12}O_{34}Cl_2Co_2Mo_8$: C 7.68, H 3.44, N 8.95, Cl 3.78, Co 6.28, Mo 40.89. Found: C 7.87, H 3.62, N 9.09, Cl 3.63, Co 6.10, Mo 40.71.

11. $[Co(C_2O_4)(en)_2]_2[MoO_4]\cdot 9H_2O$. Red crystals of **11** were obtained after 1week. Yield: 9.20 mg. Anal. calcd (%) for $C_{12}H_{50}N_8O_{21}Co_2Mo$: C 16.83, H 5.89, N 13.08, Co 13.76, Mo 11.20. Found: C 16.99, H 6.03, N 13.21, Co 13.59, Mo 11.02.

Solution based method at 110 °C

*General procedure for synthesis of compounds **1–11**.* An aqueous solution of sodium molybdate (0.5 mmol, 5 mL) and malonic acid (0.8 mmol) was added in an aqueous solution (15 mL) of the corresponding Co(III) complex (0.205 mmol) and the appropriate heteroatom source (0.043 mmol). The final reaction mixture was heated in a 30 mL Teflon-lined reactor at 110 °C for 1.5 h.

1. $[Co(C_2O_4)(NH_3)_4]_3[AlMo_6(OH)_6O_{18}]\cdot 7H_2O$. Pink-red crystals of **1** were obtained immediately after cooling the reaction mixture. Yield: 82.00 mg. Anal. calcd (%) for $C_6H_{56}N_{12}O_{43}AlCo_3Mo_6$: C 4.09, H 3.20, N 9.53, Al 1.53, Co 10.02, Mo 32.64. Found: C 3.98, H 3.11, N 9.32, Al 1.50, Co 10.10, Mo 32.56.

2. $[Co(C_2O_4)(NH_3)_4]_6[TeMo_6O_{24}]\cdot 16H_2O$. Red crystals of **2** were obtained immediately after cooling the reaction mixture. Yield: 18.00 mg. Anal. calcd (%) for $C_{12}H_{104}N_{24}O_{64}Co_6Mo_6Te$: C 5.41, H 3.93, N 12.61, Co 13.26, Mo 21.59, Te 4.79. Found: C 5.50, H 3.88, N 12.62, Co 13.05, Mo 21.55, Te 4.73.

3. $Na_2[Co(C_2O_4)(en)_2]_4[TeMo_6O_{24}]\cdot 16H_2O$. Red crystals of **3** were obtained after 2 days. Yield: 24.10 mg. Anal. calcd (%) for $C_{24}H_{96}N_{16}O_{56}Na_2Co_4Mo_6Te$: C 11.58, H 3.89, N 9.00, Na 1.85, Co 9.47, Mo 23.12, Te 5.12. Found: C 11.70, H 3.88, N 9.01, Na 1.77, Co 9.29, Mo 23.18, Te 5.06.

4. $[Co(C_2O_4)(NH_3)_4]_4[GeMo_{12}O_{40}]\cdot 6H_2O$. Red crystals of **4** were obtained immediately after cooling the reaction mixture. Yield: 79.00 mg. Anal. calcd (%) for $C_8H_{60}N_{16}O_{62}Co_4GeMo_{12}$: C 3.39, H 2.14, N 7.91, Co 8.32, Ge 2.56, Mo 40.65. Found: C 3.36, H 2.14, N 7.89, Co 8.35, Ge 2.36, Mo 40.56.

5. $[Co(C_2O_4)(NH_3)_4]_4[SiMo_{12}O_{40}]\cdot 6H_2O$. Red crystals of **5** were obtained immediately after cooling the reaction mixture. Yield: 42.45 mg. Anal. calcd (%) for $C_8H_{60}N_{16}O_{62}SiCo_4Mo_{12}$: C 3.45, H 2.17, N 8.04, Si 1.01, Co 8.46, Mo 41.30. Found: C 3.40, H 2.15, N 8.10, Si 1.05, Co 8.45, Mo 41.23.

6. $[Co(C_2O_4)(en)_2]_4[GeMo_{12}O_{40}]\cdot 12H_2O$. Red crystals of **6** were obtained after two days. Yield: 24.30 mg. Anal. calcd (%) for $C_{24}H_{88}N_{16}O_{68}Co_4GeMo_{12}$: C 9.15, H 2.82, N 7.12, Co 7.49, Ge 2.31, Mo 36.57. Found: C 9.11, H 2.88, N 7.17, Co 7.4, Ge 2.32, Mo 36.56.

7. $[Co(C_2O_4)(en)_2]_4[SiMo_{12}O_{40}]\cdot 12H_2O$. Red crystals of **7** were obtained immediately after cooling the reaction mixture. Yield: 30.80 mg. Anal. calcd (%) for $C_{24}H_{88}N_{16}O_{68}SiCo_4Mo_{12}$: C 9.29, H 2.86, N 7.22, Si 0.90, Co 7.59, Mo 37.09. Found: C 9.26, H 2.920, N 7.26, Si 0.87, Co 7.49, Mo 36.98.

8. $Na_4[Co(C_2O_4)(NH_3)_4]_3[GeMo_6O_{22}(C_3H_3O_4)_3]\cdot 7.75H_2O$. Pink crystals of **8** were obtained immediately after cooling the reaction mixture. Yield: 34.00 mg. Anal. calcd (%) for $C_{15}H_{60.5}N_{12}O_{53.75}Na_4Co_3GeMo_6$: C 8.24, H 2.79, N 7.69, Na 4.21, Co 8.09, Ge 3.32, Mo 26.33. Found: C 8.30, H 2.718, N 7.68, Na 4.23, Co 8.908, Ge 3.29, Mo 26.22.

9. $[Co(NH_3)_6][Al(C_3H_2O_4)_2(H_2O)_2](NO_3)_2{\cdot}H_2O$. Yellow-orange crystals of **9** were obtained after two days. Yield: 34.09. Anal. calcd (%) for $C_6H_{28}N_8O_{17}AlCo$: C 12.64, H 4.95, N 19.65, Al 4.73, Co 10.33. Found: C 12.62, H 5.01, N 19.62, Al 4.78, Co 10.32.

10. $[Co(en)_3]_2[Mo_8O_{26}(H_2O)_2]Cl_2{\cdot}6H_2O$. Orange crystals of **10** were obtained after one week. Yield: 25.20 mg. Anal. calcd (%) for $C_{12}H_{64}N_{12}O_{34}Cl_2Co_2Mo_8$: C 7.68, H 3.44, N 8.95, Cl 3.78, Co 6.28, Mo 40.89. Found: C 7.57, H 3.32, N 9.01, Cl 3.75, Co 6.22, Mo 40.91.

11. $[Co(C_2O_4)(en)_2]_2[MoO_4]{\cdot}9H_2O$. Red crystals of **11** were obtained immediately after cooling the reaction mixture. Yield: 19.20 mg. Anal. calcd (%) for $C_{12}H_{50}N_8O_{21}Co_2Mo$: C 16.83, H 5.89, N 13.08, Co 13.76, Mo 11.20. Found: C 16.79, H 6.00, N 13.01, Co 13.79, Mo 11.12.

Conclusions

Herein, we report mechanochemical synthesis as an unexplored yet effective method for the preparation of heteropolyoxomolybdates. Although the mechanochemical and hydrothermal syntheses yielded the same final products, the mechanochemical approach provided a valuable advantage and enabled the isolation of reaction intermediates. The PXRD data revealed that the amorphous solid rapidly converted to the final crystalline product, and validation of the PCA-derived reaction profiles confirmed that reactions were completed within 20 to 60 hours for the presented compounds. Our investigation of the catalytic activity of selected Keggin and Anderson polyoxomolybdates showed that Keggin-type polyoxomolybdates $\{SiMo_{12}O_{40}\}$ and $\{GeMo_{12}O_{40}\}$ exhibit promising photocatalytic activity for the removal of organic contaminants from wastewater under sunlight and without the need for the addition of H_2O_2.

The results also demonstrate that neither reaction temperature nor Co(III) complex cation/Mo ratio alone is sufficient to predict the outcome of polyoxomolybdate formation.

Author contributions

Conceptualization, M. C.; investigation, M. C., D. K., J. T., and V. D. (syntheses, identification, spectroscopic studies, PXRD and SCRD experiments); I. H. (Raman spectroscopy); G. M. (catalytic activity); T. H., quantum chemical calculations; writing – original draft preparation, M. C., D. K., V. D., and I. H. part of Raman spectroscopy; G. M. part of catalytic study; T. H. part of quantum chemical calculations; project administration, V. V.; funding acquisition, V. V.; M. C. and V. V. review and editing. All authors have read and agreed to the published version of the manuscript.

Conflicts of interest

There are no conflicts to declare.

Data availability

The data supporting this article have been included as part of the supplementary information (SI). Supplementary information is available. See DOI: https://doi.org/10.1039/d5dt03064a.

Crystallographic information files are available from the Cambridge Crystallographic Data Centre (CCDC) upon request (http://www.ccdc.cam.ac.uk, CCDC deposition numbers 2514646–2514656).[55a–k]

Acknowledgements

This work was supported by the Croatian Science Foundation under the project number HRZZ-IP-2022-10-7368 and HRZZ-DOK-NPOO-2023-10-2405. We acknowledge the support of the project CIuK co-financed by the Croatian Government and the European Union through the European Regional Development Fund-Competitiveness and Cohesion Operational Programme (Grant KK.01.1.1.02.0016).

References

1 K. S. Asha, R. Bhattacharjee and S. Mandal, *Angew. Chem., Int. Ed.*, 2016, **55**, 11528.
2 J. He, N. W. Waggoner, S. G. Dunning, A. Steiner, V. M. Lynch and S. M. Humphrey, *Angew. Chem., Int. Ed.*, 2016, **55**, 12351.
3 X. F. Lu, P. Q. Liao, J. W. Wang, J. X. Wu, X. W. Chen, C. T. He, J. P. Zhang, G. R. Li and X. M. Chen, *J. Am. Chem. Soc.*, 2016, **138**, 8336.
4 D. J. Levine, T. Runčevski, M. T. Kapelewski, B. K. Keitz, J. Oktawiec, D. A. Reed, J. A. Mason, H. Z. H. Jiang, K. A. Colwell, C. M. Legendre, S. A. FitzGerald and J. R. Long, *J. Am. Chem. Soc.*, 2016, **138**, 10143.
5 D. Kim, D. R. Whang and S. Y. Park, *J. Am. Chem. Soc.*, 2016, **138**, 8698.
6 R. J. Comito, K. J. Fritzsching, B. J. Sundell, K. Schmidt-Rohr and M. Dincă, *J. Am. Chem. Soc.*, 2016, **138**, 10232.
7 M. H. Zeng, Z. Yin, Z. H. Liu, H. B. Xu, Y. C. Feng, Y. Q. Hu, L. X. Chang, Y. X. Zhang, J. Huang and M. Kurmoo, *Angew. Chem., Int. Ed.*, 2016, **55**, 11407.
8 B. Zhong, J. Liu, G. Liu, Z. Zhang, J. Chen and X. Wang, *J. Mol. Struct.*, 2025, **1332**, 141679.
9 C. Lian, S.-H. Zhao, H.-L. Li and X. Cao, *Chin. Chem. Lett.*, 2024, **35**, 109343.
10 A. Gao, S.-H. Zhao, J. Wang and H.-L. Li, *Rev. Inorg. Chem.*, 2025, DOI: 10.1515/revic-2025-0047.
11 X. Li, W. Guo, Z. Liu, R. Wang and H. Liu, *Appl. Surf. Sci.*, 2016, **369**, 130.
12 Y. L. Hou, R. W. Y. Sun, X. P. Zhou, J. H. Wang and D. Li, *Chem. Commun.*, 2014, **50**, 2295.
13 C. Wang, F. Xing, Y. L. Bai, Y. Zhao, M. X. Li and S. Zhu, *Cryst. Growth Des.*, 2016, **16**, 2277.
14 Y. P. Wu, X. Q. Wu, J. F. Wang, J. Zhao, W. W. Dong, D. S. Li and Q. C. Zhang, *Cryst. Growth Des.*, 2016, **16**, 2309.

15 M. S. Deenadayalan, N. Sharma, P. K. Verma and C. M. Nagaraja, *Inorg. Chem.*, 2016, **55**, 5320.
16 S. Parsons, *Advanced Oxidative Processes for Water and Wastewater Treatment*, IWA Publishing, UK, 2004.
17 H. Gerixhac, *Electrochim. Acta*, 1993, **38**, 39.
18 R. W. Mathews, *J. Catal.*, 1988, **111**, 264.
19 A. L. Pruden and D. F. Ollis, *J. Catal.*, 1983, **82**, 404.
20 C. Streb, *Dalton Trans.*, 2012, **41**, 1651.
21 E. Papaconstantinou, *Chem. Soc. Rev.*, 1989, **18**, 1.
22 D. Kuzman, V. Damjanović, V. Stilinović, M. Cindrić and V. Vrdoljak, *New J. Chem.*, 2021, **45**, 19764.
23 D. Kuzman, M. Pajić, L. Drempetić, J. Sarjanović, J. Pisk, T. Hrenar, M. Cindrić and V. Vrdoljak, *ACS Omega*, 2025, **10**, 16668.
24 M. Cindrić, N. Strukan and V. Vrdoljak, *Croat. Chem. Acta*, 1999, **72**, 501–509.
25 M. Cindrić, N. Strukan, V. Vrdoljak, M. Devčić, Z. Veksli and B. Kamenar, *Inorg. Chim. Acta*, 2000, **304**, 260–267.
26 M. Cindrić, N. Strukan, V. Vrdoljak, T. Fuss, G. Giester and B. Kamenar, *Inorg. Chim. Acta*, 2000, **309**, 77–81.
27 P. Roman, A. Lique, J. M. Gutiérrez-Zorrilla and S. Garcia-Granada, *Polyhedron*, 1991, **10**, 2057.
28 P. Román, A. Lique, C. Guzmán-Miralles and J. I. Beitia, *Polyhedron*, 1995, **14**, 2863–2869.
29 Y. Chen, X. Shen, H. Zhang, C. Huang, Y. Cao and R. Sun, *Vib. Spectrosc.*, 2006, **40**, 142–147.
30 G. Mahata and K. Biradha, *Inorg. Chim. Acta*, 2007, **360**, 281–285.
31 R. P. Sharma, R. Bala, R. Sharma and P. Venugopalan, *J. Coord. Chem.*, 2004, **57**, 1563–1569.
32 S. Ikegami and A. Yagasaki, *Materials*, 2009, **2**, 869–875.
33 E. M. McCarron, J. F. Whitney and D. B. Chase, *Inorg. Chem.*, 1984, **23**, 3275–3280.
34 H.-Y. Zang, K. Tan, W. Guan, S.-L. Li, G.-S. Yang, K.-Z. Shao, L.-K. Yan and Z.-M. Su, *CrystEngComm*, 2010, **12**, 3684–3690.
35 N. Laronze, J. Marrot and G. Hervé, *Chem. Commun.*, 2003, 2360–2361.
36 M. Tahmasebi, M. Mirzaei, H. Eshtiagh-Hosseini, J. T. Mague, A. Bauzá and A. Frontera, *Acta Crystallogr., Sect. C: Struct. Chem.*, 2019, **75**, 469–477.
37 M. Tahmasebi, M. Mirzaei, M. M. Matin, S. Iranpour and J. T. Mague, *J. Mol. Struct.*, 2022, **1247**, 131401.
38 V. Damjanović, J. Pisk, D. Kuzman, D. Agustin, V. Vrdoljak, V. Stilinović and M. Cindrić, *Dalton Trans.*, 2019, **27**, 9974–9983.
39 A. Tapparo, S. L. Heath, P. A. Jordan, G. R. Moore and A. K. Powell, *J. Chem. Soc., Dalton Trans.*, 1996, **8**, 1601–1606.
40 P. Wu, Y. Wang, B. Huang and Z. Xiao, *Nanoscale*, 2021, **13**, 7119–7133.
41 J. Pisk, T. Hrenar, M. Rubčić, G. Pavlović, V. Damjanović, J. Lovrić, M. Cindrić and V. Vrdoljak, *CrystEngComm*, 2018, **20**, 1804–1817.
42 N. Hur, W. G. Klemperer and R. C. Wang, *Inorganic Synthesis*, JohnWiley&Sons, NewYork, 1990, vol. 27, p. 77.
43 T. Degen, M. Sadki, E. Bron, U. König and G. Nénert, The HighScore suite, *Powder Diffr.*, 2014, **29**, S13–S18.
44 Agilent, *CrysAlis PRO 2014; Oxford Diffraction, Xcalibur CCD System, CrysAlis CCD and CrysAlis RED software, Version 1.170*, Agilent Technologies Ltd., Yarnton, Oxfordshire, England, 2003.
45 G. M. Sheldrick, SHELXT-Integrated Space-Group and Crystal-Structure Determination, *Acta Crystallogr., Sect. A: Found. Adv.*, 2015, **71**, 3–8.
46 A. L. Spek, Structure validation in chemical crystallography, *Acta Crystallogr., Sect. D: Biol. Crystallogr.*, 2009, **65**, 148–155.
47 C. F. Macrae, P. R. Edgington, P. McCabe, E. Pidcock, G. P. Shields, R. M. Taylor, M. Towler and J. van de Streek, Mercury 4.0: from visualization to analysis, design and prediction, *J. Appl. Crystallogr.*, 2020, **53**, 226–235.
48 E. Beltrami, *Giornale di Matematiche ad Uso degli Studenti Delle Universita*, 1873, vol. 11, p. 98.
49 K. Pearson, *Philos. Mag.*, 1901, **2**, 559.
50 H. Hotelling, *J. Educ. Psychol.*, 1933, **24**, 417.
51 I. T. Jolliffe, *Principal Component Analysis*, Springer, Berlin, 1986.
52 O. Jović, T. Smolić, I. Primožič and T. Hrenar, *Anal. Chem.*, 2016, **88**, 4516.
53 T. Hrenar, I. Primožič, D. Fijan and M. Majerić Elenkov, *Phys. Chem. Chem. Phys.*, 2017, **19**, 31706–31713.
54 D. Raljević, J. Parlov Vuković, V. Smrečki, L. J. Marinić Pajc, P. Novak, T. Hrenar, T. Jednačak, L. Konjević, B. Pinević and T. Gašparac, *Fuel*, 2021, **305**, 121561.
55 (*a*) CCDC 2514646: Experimental Crystal Structure Determination, 2026, DOI: 10.5517/ccdc.csd.cc2qdpmg; (*b*) CCDC 2514647: Experimental Crystal Structure Determination, 2026, DOI: 10.5517/ccdc.csd.cc2qdpnh; (*c*) CCDC 2514648: Experimental Crystal Structure Determination, 2026, DOI: 10.5517/ccdc.csd.cc2qdppj; (*d*) CCDC 2514649: Experimental Crystal Structure Determination, 2026, DOI: 10.5517/ccdc.csd.cc2qdpqk; (*e*) CCDC 2514650: Experimental Crystal Structure Determination, 2026, DOI: 10.5517/ccdc.csd.cc2qdprl; (*f*) CCDC 2514651: Experimental Crystal Structure Determination, 2026, DOI: 10.5517/ccdc.csd.cc2qdpsm; (*g*) CCDC 2514652: Experimental Crystal Structure Determination, 2026, DOI: 10.5517/ccdc.csd.cc2qdptn; (*h*) CCDC 2514653: Experimental Crystal Structure Determination, 2026, DOI: 10.5517/ccdc.csd.cc2qdpvp; (*i*) CCDC 2514654: Experimental Crystal Structure Determination, 2026, DOI: 10.5517/ccdc.csd.cc2qdpwq; (*j*) CCDC 2514655: Experimental Crystal Structure Determination, 2026, DOI: 10.5517/ccdc.csd.cc2qdpxr; (*k*) CCDC 2514656: Experimental Crystal Structure Determination, 2026, DOI: 10.5517/ccdc.csd.cc2qdpys.